- Publisher source acknowledgment:
https://doi.org/10.1016/j.ejmech.2022.114240 (final version)

Synthesis and antitumor properties of new indole and pyranoindole derivatives

Domenico Iacopetta[a,1], Alessia Catalano[b,1], Jessica Ceramella[a], Alexia Barbarossa[b], Alessia Carocci[b,*], Alessia Fazio[a], Chiara Latorre[a], Anna Caruso[a], Marco Ponassi[c], Camillo Rosano[c], Carlo Franchini[b], Maria Stefania Sinicropi[a]

[a]*Department of Pharmacy, Health and Nutritional Sciences, University of Calabria, 87036, Arcavacata di Rende (Italy)*

[b]*Department of Pharmacy-Drug Sciences, University of Bari "Aldo Moro", 70126, Bari (Italy)*

[c]*Biopolymers and Proteomics IRCCS, Ospedale Policlinico San Martino–IST, Largo R. Benzi 10, 16132 Genova, Italy*

[*] *Corresponding author: e-mail address: alessia.carocci@uniba.it*

[1] *These authors equally contributed to this work.*

Abstract

The indole scaffold has been recognized, over the years, as a model for the synthesis of compounds with anticancer activity by dint of its substantiated ability to act via multiple mechanisms, which also involve the inhibition of enzymes engaged in DNA replication. In this regard, a new series of indole and pyranoindole derivatives have been prepared, some of which showed good antitumor activity and proved their inhibitory effects on the tubulin target. The antitumor activity of the newly synthesized compounds has been evaluated on breast cancer cell lines, as MCF-7 and MDA-MB231, tumoral cervical cells line HeLa and Ishikawa endometrial cell line. Among the compounds under study, **7** exhibited a good antitumor activity on HeLa cell line (IC_{50}=7.20 μM), leading to cell death by apoptosis due to the inhibition of tubulin polymerization, which demonstrated that the compound can explicate its function in a similar way to Vinblastine, a well-known inhibitor of tubulin polymerization. The data were also confirmed by *in silico* assays. No cytotoxicity against non-tumoral cells has been detected. Furthermore, in order to suggest a possible relationship between anticancer effects and antioxidant properties, DPPH and ABTS tests were performed, together with fluorescence assays on 3T3-L1 cells. All our findings taken together led us to consider compound **7** a favourable candidate for the battle against cancer.

Key words: indole derivatives, tubulin, molecular docking studies, anticancers, antioxidants

Introduction

Despite the technological and social development, tumor is one of the most common diseases of concern and a leading cause of human suffering. It was estimated that deaths from cancer worldwide would rise over 13.1 million in 2030 (WHO report, Globocan 2012, IARC). Therefore, the design of newer and potent anticancer agents with higher selectivity on neoplastic cells and few side effects, able to overcome problems like severe toxicity as well as resistance with the existing drugs, may be envisaged. An ongoing source of debate is the possibility of some molecules with antioxidant properties to explicate chemopreventive action. Indeed, many prior studies corroborate that the antioxidants can enhance the known chemotherapy protocols by ameliorating the toxic side effects without affecting treatment efficacy[1]. Besides, other *in vitro* investigations suggest the relevant role of this kind of molecules in inducing the apoptosis in cancer cells[2]. In the last decades, research efforts resulted in the development of numerous antineoplastic agents with a variety of structures. Among them, the indole nucleus, due to its biodiversity and versatility, has been a highly privileged motif for the target-based design and development of anticancer agents[3]. Furthermore, some of naturally occurring indole alkaloids, including vincristine, vinblastine, vinorelbine and vindesine, have gained FDA approval for anti-tumor activity. Taking inspiration from these natural compounds, several synthetic analogues were synthesized, some of which showing good anti-tumor activity[4]. Recently, indole derivatives have been studied as inhibitors of enzymes involved in DNA replication as topoisomerase, telomerase, tubulin[5-7]. Due to the multiple functions of microtubules in cell mitosis, tubulin has become a highly attractive target for new anticancer drugs discovery[8]. Therefore, tubulin/microtubule-interacting drugs are used successfully for treatment of a wide variety of human cancers[9]. In the last decade, the synthesis and biological evaluation of some indole and corresponding pyranoindole derivatives (**I–IV,** Figure 1) was reported[10]. The compounds were evaluated for their inhibition of NO production, antioxidant activity and for their ability to inhibit *in vitro* the growth of four human tumor cell lines. Two indole derivatives (**I, II**) showed to be active against amelanotic melanoma cell lines, while inhibiting NO production in murine monocytic

macrophage. Based on these evidences, new indole and pyranoindole derivatives (**5–13,** Figure 2) have been synthesized in order to enlarge studies on this class of compounds. The antiproliferative activity on breast cancer and human ovarian carcinoma cell lines of these new compounds is reported herein, along with the evaluation of their ability to inhibit tubulin microtubule polymerization. Furthermore, in order to delve into the possible relationship between the antioxidant properties and anticancer mechanisms, the antioxidant activity of the synthesized compounds have been evaluated by means of both *in vitro* and cellular assay. Finally, molecular docking studies have also been conducted to support the results obtained.

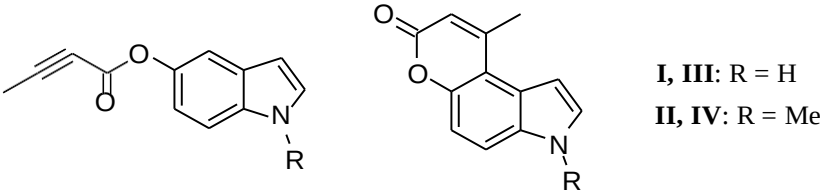

I, II **III, IV**

Figure 1. Structure of indoles (**I, II**) and pyranoindoles (**III, IV**) described in the literature

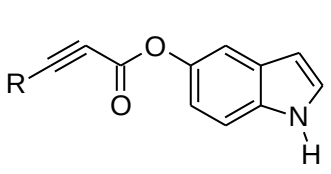

5: R = CH_2CH_3
6: R = $CH_2CH_2CH_3$
7: R = Ph

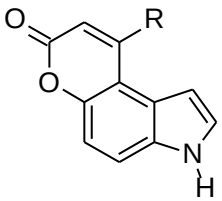

11: R = $CH(CH_3)_2$
12: R = $CH_2CH_2CH_3$

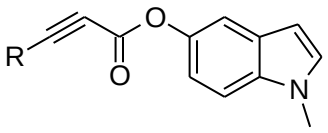

8: R = CH_2CH_3
9: R = $CH(CH_3)CH_2CH_3$
10: R = Ph

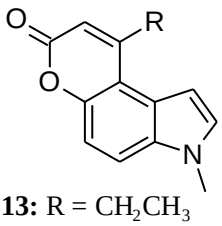

13: R = CH_2CH_3

Figure 2. Structure of indoles **(5–10)** and pyranoindoles **(11–13)** under study.

2. Results and Discussion

2.1. Chemistry

The synthesis of 5-hydroxy-1-methylindole **3** is depicted in Scheme 1. 5-Methoxyindole **1** was treated with NaH to obtain the *N*-anion followed by reaction with methyl iodide to give 5-methoxy-1-methylindole **2**. Selective demethylation of the methoxy group by heating under reflux in anhydrous pyridine hydrochloride gave the desired **3**.

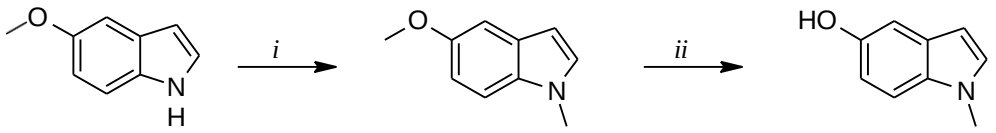

1 **2** **3**

Scheme 1. *Reagents and conditions*: (i) NaH 60% oil dispersion, CH_3I, DMF, 0 °C→rt, 1 h; (ii) pyridine hydrochloride, reflux, 3 h.

The synthesis of the indole and pyranoindole derivatives is depicted in Scheme 2. Commercial 5-hydroxyindole **4** was submitted to esterification with pent-2-ynoic acid, es-2-ynoic acid or phenylpropiolic acid to give the corresponding esters **5, 6, 7**, respectively. The same reactions, run on 5-hydroxy-1-methylindole **3** gave esters **8, 9, 10**. When esters **5, 6, 8** were heated under reflux in dioxane-dichloroethane in the presence of $PtCl_4$ as a catalyst, an intramolecular cyclization occurred giving pyranoindoles **11,12,13**, respectively.

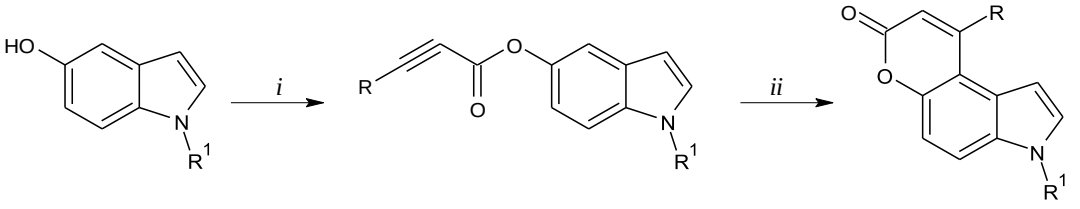

3,4 **5-10** **11-13**

4-7,11,12: R^1 = H
3,8-10,13: R^1 = Me
5,8,11,13: R = Me
6,9,12: R = *n*-Pr
7,10: R = Ph

Scheme 2. *Reagents and conditions*: (i) pent-2-ynoic acid (for compounds **5** and **8**) or es-2-ynoic acid (for compounds **6** and **9**) or phenylpropiolic acid (for compounds **7** and **10**), DCC, DMAP, CH_2Cl_2/DMF (10:1), rt, 4 h; (*ii*) $PtCl_4$, 1,4-dioxane/1,2-dicloroethane (1:1), reflux, 5 h.

2.1.1 Thermal stability test

Prior research has thoroughly investigated the possibility of several organic compounds to decompose by heat action[11]. Compound **7**, the most active molecule of the series, presents in its structure a triple bond, a possible source of molecular instability. For this reason, through the modification of already known protocols aimed at verifying heat stability, we performed a "stress test assay" on **7** by heating it for 6 hours at 60 °C. At the end of the process, we compared the NMR spectra of **7** in the usual conditions and after the heat treatment. The match of the two spectra surmises that **7** is heat-resistant.

2.2. Biological Results

2.2.1 Antitumor activity

The cytotoxic activities of synthesized compounds were evaluated against four human cancer cell lines, including two breast cancer cells (MCF-7 and MDA-MB-231) and two human uterine cancer cells (HeLa and Ishikawa), using MTT assay. The calculated IC_{50} values of studied compounds in comparison with the reference drug, Vinblastine, are listed in Table 1. Among them, the indole bearing the phenylpropiolic group, compound **7**, exhibited the best antitumor activity, particularly toward the human cervical cancer cells HeLa and the breast cancer cells MCF-7, with the IC_{50} values amounting to 3.6±0.5 and 3.8±0.7 μM, respectively. A moderate antitumor activity toward all the cell lines used was also shown by compounds **5** and **6**, mostly toward HeLa cells (IC_{50}= 9.8±0.3 and 14.5±0.6 μM, respectively). Compounds **5** and **6** are structurally the indole analogues of compound **7**, bearing the pent-2-ynoyl and es-2-ynoyl groups, respectively. The methylindole derivatives **8**, **9** and **10** possessed a lower activity than the indole analogues, except for methylindole **8** that showed an interesting antitumor activity, in particular against the uterine cancer cells Ishikawa and HeLa

(IC_{50}= 13.1±0.3 and 14.0±0.7 μM, respectively). Thus, the addition of a methyl group on the nitrogen indole ring appears to cause a decrease in antitumor activity. Moreover, the pyranoindole compounds **11**, **12** and **13** exhibited a lower o no antitumor activity on the cell lines tested, highlighting the importance of the indole group in the moiety of these compounds. The known microtubule-binding agent Vinblastine showed a stronger anti-proliferative activity than our synthesized compounds on all cancer cell lines, with IC_{50} values between $2.3x10^{-2}$±0.6 μM and $1.6x10^{-1}$±0.3 μM. However, Vinblastine exhibited also a dramatic cytotoxic effect on normal cells used in this assay (MCF-10A and Hek-293), unlike our compounds that did not interfere with the non-tumoral cells viability, at least until the concentration of 200 μM and under the conditions used for this assay.

Table 1. IC_{50} values of compounds **5-13** and Vinblastine expressed in μM.

Compounds	MCF-7	MDA-MB-231	HeLa	Ishikawa	MCF-10A	Hek-293	3T3-L1
5	13.1±0.3	10.7±0.2	9.8±0.3	12.1±0.6	>200	>200	>200
6	30.2±0.2	15.9±0.5	14.5±0.6	30.5±0.5	>200	>200	>200
7	3.8±0.7	9.9±0.3	3.6±0.5	10.1±0.7	>200	>200	>200
8	23.0±0.4	23.5±0.4	14.0±0.7	13.1±0.3	>200	>200	>200
9	>200	>200	>200	>200	>200	>200	>200
10	37.6±0.5	40.7±0.8	49.5±0.9	77.7±0.4	>200	>200	>200
11	86.0±0.3	44.4±0.3	21.1±0.7	84.0±0.5	>200	>200	>200
12	>200	172.4±0.6	141.4±0.7	>200	>200	>200	>200
13	131.5±0.3	80.2±0.5	>200	>200	>200	>200	>200
Vinblastine	$4.5x10^{-2}$±0.6	$1.6x10^{-1}$±0.3	$6.7x10^{-2}$±0.5	$2.5x10^{-2}$±0,7	$2.3x10^{-2}$±0.6	80.8±0.4	$1.9x10^{-4}$±0.8

*2.2.2 Effect of compound **7** on microtubule dynamics and cell death by apoptosis*

Numerous studies have shown that the alteration of microtubule dynamics induced by different compounds causes mitochondrial membrane potential activation, cell cycle and mitotic process arrest [9, 12-14]. To demonstrate the specific action of the synthesized compounds on tubulin network, we

chose compound **7** and performed an immunofluorescence test using the anti-β-tubulin antibody on HeLa cells, on which compound **7** displayed the best antitumor activity. In Figure 3, the vehicle-treated cells (panel A, CTRL) showed a normal distribution of the microtubule network, with intact tubulin polymers regularly distributed throughout the cytoplasmic region (panel B, CTRL). After only 24 hours of compound **7** treatment (used at its IC_{50} value), tubulin microfilaments appeared as distinct punctiform structures and accumulates unfairly throughout the cell cytoplasm and nucleus (Panel B, compound **7**, see white arrows). A similar behavior can be observed in Figure 3, Panel B, Vinblastine, where microtubules became irregular and the arrangement and organization of the tubulin network showed a severe disruption with a stronger formation of dot-like structures.

FIGURE 3

To confirm these data, we examined the effect of compound **7** on the tubulin polymerization using a specific *in vitro* assay and measuring the turbidity variation every 30 seconds at 350 nm for 90 minutes. We used two well-known compounds as reference molecules, a tubulin polymerization inhibitor, Vinblastine, and a stabilizing agent, Paclitaxel. In the only vehicle (CTRL) reaction, tubulin heterodimers rapidly self-assembled to form linear tubulin polymers, in a time-dependent manner, with a final optical density (OD_{350}) of above 0.44, as showed in Figure 4. The microtubule-stabilizing agent Paclitaxel caused an increased rate of tubulin heterodimers assembly, whereas using the microubule-destabilizing agent such Vinblastine, the polymerization reaction was hampered (final OD_{350} of 0.19). Compound **7** interfered with the tubulin polymerization similarly to Vinblastine, indeed the polymerization curve reached the steady state at an OD_{350} 1.5-fold lesser than the control reaction (OD_{350} = 0.48 and 0.3 for CTRL and compound **7**, respectively), with a final OD_{350} value of about 0.24. Thus, compound **7** resulted an inhibitor of tubulin polymerization.

FIGURE 4

The alteration of microtubules network causes a blockage of the mitotic process progression with the induction, in the last phase, of the apoptotic process [15-16]. For this reason, we decided to perform a TUNEL assay with the aim to demonstrate the ability of compound **7** to induce cell death by apoptosis on the HeLa tumor cell line. The induction of apoptosis promotes morphological characteristic changes such as the cellular narrowing (the cytoplasm is dense and the organelles are narrower), the picnosis, which is the result of the condensation of the chromatin, and the fragmentation of the DNA[17]. The experiment was conducted by treating HeLa with compound **7**, used at its IC_{50} value, or with the vehicle (DMSO) for 24 h, and then performing the TUNEL assay, as described in the materials and methods section. The images obtained (Figure 5) clearly show the development of a nuclear green fluorescence in the cells treated with compound **7**, due to DNA damage related to the apoptotic process. This fluorescence, however, is absent in the cells treated with the vehicle only (Panel B, CTRL) used as control.

FIGURE 5

It is known that reactive oxygen species (ROS), at low doses, are essential for regulation of normal physiological functions of the cells. However, high cellular levels of ROS cause serious damages to proteins, nucleic acids, lipids, membranes and others organelles, which can lead to trigger cell death pathway such as apoptosis [18]. Considering the main role of ROS in the regulation of the apoptosis process, we investigated whether the most active compound **7**could act as ROS scavenger in a non-tumoral cell model, the mouse fibroblasts 3T3-L1, by using fluorescence assays. In particular, we treated 3T3-L1 with compound **7** at a concentration of 10 μM for 24 h and then we induced ROS production treating with menadione (Men) for 1 h at 40 μM. At the end of the treatment cells were incubated with 2',7'-dichlorofluorescein diacetate (DCFH-DA) for 2 h. DCFH-DA is hydrolyzed by cellular esterases to 2',7'-dichlorodihydrofluorescein and, then, oxidized to the green fluorescent 2',7'- dichlorofluorescein (DCF) by intracellular H_2O_2. The green fluorescence was then observed

and imaged under a fluorescence microscope. The obtained results, showed in Figure 6, highlighted that the pre-treatment with compound **7** significantly reduced the oxidative stress induced by menadione (Figure 6a, panel B, **7**+Men), if compared with the cells treated only with menadione (Figure 6a, panel B, Men). The quantification of the green fluorescence (Figure 6b) demonstrated, in fact, that compound **7** was able to cause a three-fold decrease of ROS generation in the 3T3-L1 cells, acting as a good scavenging of ROS.

FIGURE 6

2.3 In vitro antioxidant activity

The radical scavenging activity of the synthesized compounds against the two most commonly used stable radicals (DPPH• and $ABTS^{\bullet+}$) was evaluated by *in vitro* studies.

2.3.1 DPPH assay

The free radical scavenging activity against DPPH was determined for all compounds under study (**5-13**). The DPPH assay, which is based on the reduction of the purple DPPH to 1, 1-diphenyl-2-picryl hydrazine (DPPH-H) via hydrogen transfer (HT) mechanisms, measures the ability of antioxidant compounds for trapping free radicals by donating hydrogen atoms, producing in consequence the bleaching of the colored radical solutions.

The results obtained as a function of concentration (8.33, 3.33, 1.67, 0.33 μg mL^{-1}) were reported in Table 2 and Figure 7. The results showed that the scavenging effects of the compounds on DPPH radical increased with the concentration. The data indicated that, among the synthetic compounds, **6** with the inhibition percentage of 90.45% at the highest concentration (8.33 μg mL^{-1}), displayed higher antioxidant activity than the other compounds. Compound **6** exhibited a high value of antioxidant ability even at lower concentration (78.2% at 1.67 μg mL^{-1}). Compounds **9** and **10** showed moderate antioxidant activities (79.04 and 73.40 %, respectively, at the highest concentration).

Compounds **7** and **12** showed a DPPH inhibition percentage of 43% and 50% at the highest concentration. The lowest antioxidant activity with a DPPH inhibition value of 10% at 8.33 μg mL^{-1}

belongs to **8**. Compound **11** was the only compound that did not exhibit any antioxidant activity at the lowest concentration tested (0.33 μg mL^{-1}).

Table 2. $\%I_{DPPH}$ of compounds **5–13** ± standard deviation

	Concentration (μg mL^{-1})			
Compound	**8.33**	**3.33**	**1.67**	**0.33**
Trolox	99.0±0	93.33±0.51	92.68±0.53	92.68±0.53
5	36.02±0.78	32.02±2.85	30.13±0.69	17.75±0.53
6	90.45±0.52	87.96±1.06	78.18±0.54	24.90±2.98
7	43.25±1.36	31.42±3.48	26.58±3.52	5.96±1.35
8	10.44±1.61	6.93±1.22	4.81±0.76	2.02±0.76
9	79.04±2.69	49.11±1.68	35.00±2.14	11.83±3.65
10	73.40±0.30	42.96±3.08	24.76±4.69	11.80±0.45
11	35.60±2.21	26.83±1.47	11.23±0.41	0
12	50.53±0.25	37.72±3.27	28.16±1.38	21.48±0.40
13	14.39±1.66	15.25±0.90	13.16±0.25	9.55±2.79

FIGURE 7

Antioxidant capacities were also expressed as Trolox equivalent antioxidant capacity (TEAC). The results reported in Table 3 highlighted that **6** was the compound with the highest antioxidant activity

at all concentrations (from 37.90±8.25 at 0.33 µg mL^{-1} to 219.56±1.43 at 8.33 µg mL^{-1}), while lowest TEAC value results from **8** (2.90±0.02 at 8.33 µg mL^{-1}).

Table 3. DPPH radical scavenging of compounds **5–13** expressed as µg of TE/g DW

	Concentration (µg mL^{-1})			
Compound	**8.33**	**3.33**	**1.67**	**0.33**
5	70.05±2.17	59.08±7.87	53.86±1.89	19.81±1.49
6	219.56±1.43	212.67±2.96	185.52±1.48	37.90±8.25
7	89.56±3.78	43.60±9.74	56.94±9.58	0
8	2.90±0.02	0	0	0
9	189.09±7.28	107.91±4.58	69.56±5.85	6.70±0.89
10	173.62±0.81	90.75±8.36	41.22±12.77	6.00±1.24
11	71.23±5.98	47.43±3.96	5.05±1.08	0
12	111.71±0.70	76.94±8.86	51.00±0.14	32.90±1.08
13	13.62±4.54	16.00±2.46	10.29±0.72	0.51±0.02

In order to furtherly assess which extracts have the greatest antioxidant activity, EC_{50} values were determined (Table 4). Low EC_{50} values reflect a strong ability of the molecule to act as a DPPH scavenger whereas a high EC_{50} value indicates low scavenging activity of the scavengers, as more amount of the scavengers was required to achieve 50 % scavenging reaction. As a consequence, the scavengers are less effective at scavenging DPPH radicals. Data obtained showed that the order of reactivity found was **6** > **9** > **10** > **12** > **7** > **5** >**11** > **13** > **8**. Considering these findings, it is possible to confirm that the compound **6** is the compound with the highest DPPH radical scavenging capacity while the compound **8** is a poor DPPH radical scavenger.

Table 4. EC_{50} values of compounds **5–13** expressed in μg mL^{-1} ± standard deviation

Compound	EC_{50}± SD
Trolox	0.04±0.01
5	8.67 ± 1.21
6	0.66 ± 0.2
7	8.30 ± 2.43
8	61.76 ± 2.36
9	2.96 ± 0.54
10	4.00 ± 0.12
11	12.79 ± 1.17
12	5.76 ± 1.32
13	32.55 ± 1.41

2.3.2 ABTS assay

The free radical scavenging activity against ABTS (2,2'-azino-bis(3-ethylbenzothiazoline-6-sulfonate)) was determined at four different concentrations (2.5, 1.0, 0.5 and 0.1 mg mL^{-1} in DMSO). All the derivatives exhibited a lower capacity to inhibit the cationic radical $ABTS^{\bullet+}$ than the DPPH radical (Table 5 and Figure 8). Similarly to-DPPH assay, the scavenging effects of the compounds on cationic radical $ABTS^{\bullet+}$ increased with the compound concentration. An opposite trend was observed for the ABTS assay, where **9** and **10** had higher scavenging activity (30.34% and 21.56, respectively) than **6** (14.96%). The antioxidant ability determined by *in vitro* assays can significantly differ[19] but the combination of the results obtained from these two assays is considered of higher significance for a reliable evaluation of compounds radical scavenging capacity than the use of only one method. The ABTS assay is based on the *in situ* generation of a blue/green radical ($ABTS^{\bullet+}$) that can be reduced by antioxidants by either single electron transfer (SET) or hydrogen transfer (HT) mechanisms,

whereas the DPPH assay is based on its reduction to 1,1-diphenyl-2-picryl hydrazine (DPPH-H) via HT mechanism.

6 at the highest concentration did not exceed 15 % of inhibitory activity, while recording the zero at the lowest concentration. For all the other tested molecules no important inhibitory activity was highlighted and **11, 8, 13** were confirmed as the least active compounds also against the radical cation ABTS$^{\bullet+}$.

Table 5. %I_{ABTS} of compounds **5–13** ± standard deviation

	Concentration (μg mL^{-1})			
Compound	**25**	**10**	**5**	**1**
Trolox	99.00±0	99.04±0.41	51.52±1.33	18.81±0.65
5	4.82±0.48	3.12±0.51	2.36±0.28	1.18±0.69
6	14.96±0.33	3.43±0.33	2.36±0.07	0
7	11.59±0.16	5.89±0.70	4.62±0.33	0.58±0.02
8	3.52±1.56	3.13±1.17	2±0.73	0
9	30.34±1.35	15.98±1.96	6.86±0.57	2.85±2.01
10	21.56±1.48	8.86±1.38	3.81±0.28	1.67±0.51
11	1.26±0.24	0	0	0
12	5.25±0.27	4.12±0.66	3.22±0.14	0.59±0.38
13	2.51±0.5	0.51±0.03	0	0

FIGURE 8

Antioxidant capacities were also expressed as Trolox equivalent antioxidant capacity (TEAC) (Table 6). The results highlighted that the values were very low even for the **9** which showed the highest ABTS inhibition percentage among all the compounds (2.07% at 8.33 μg mL^{-1}).

Table 6. ABTS radical scavenging of compounds **5–13** expressed as µg of TE/g DW

	Concentration (µg mL^{-1})			
Compounds	**25**	**10**	**5**	**1**
5	0.34±0.04	0.21±0.04	0.16±0.02	0.07±0.04
6	1.10±0.02	0.23±0.02	0.15±0.01	0
7	0.63±0.01	0.17±0.06	0.07±0.03	0.58±0.02
8	0.31±0.12	0.28±0.09	0.18±0.06	0
9	2.07±0.11	0.94±0.16	0.22±0.03	0
10	1.67±0.11	0.71±0.11	0.33±0.01	0.17±0.10
11	0.07±0.02	0	0	0
12	0.07±0.02	4.12±0.66	3.22±0.14	0.59±0.38
13	0.22±0.18	0.07±0.08	0.03±0	0.03±0

The EC_{50} values for the ABTS inhibition percentage are shown in Table 7. Data highlighted that the order of compound reactivity was **9** >**10** > **6** > **12** > **7**> **9** >**8**> >**13** > **11**, thus **9** and **11** are the compounds with the highest and lowest ABTS radical scavenging, respectively.

Table 7. EC_{50} values expressed in μg mL^{-1} ± standard deviations

Molecules	EC_{50}± DS
Trolox	2.20±0.12
5	435.5 ± 0.5
6	156.6 ± 0.7
7	178.5 ± 1.0
8	560.5 ± 0.9
9	54.96 ± 1.48
10	92.33 ± 1.16
11	2494 ± 1
12	377 ± 1
13	1436 ± 1

2.4 Docking Studies

To select among our compounds the best lead candidates and to identify their possible binding modes to human tubulin, we performed different docking simulations using as a target the atomic structures of the polymeric complex formed between Tubulin α, Tubulin β, Stathmin4 and the Tubulin Tyrosine Ligase[20] [PDB code 5J2T]. We compared the binding modes or our moieties to the ones of the known ligands Colchicine and Vinblastine (Figure 9). For all our molecules, we performed a "blind docking": *i.e.* the docking of small molecules to their targets was done without a priori knowledge of the binding mode of the ligand in the active site of the protein. Our procedure was firstly validated by correctly positioning Vinblastine in its correct binding site, with a RMSD of less than 0.2 Å with respect to the one determined by X-ray crystallography.

The binding site of our moieties is placed on the interface between the alfa and beta subunit of the quaternary assembly of tubulin, in a cleft placed about 7.5Å far from the Vinblastine binding site. Table 8 reports the residues involved in ligand binding and the binding energies of all the complexes formed by tubulin and our compounds.

Table 8. Binding energies of the complexes formed by tubulin and compounds **5-13** and residues involved in ligand binding.

Compound	**Binding Energy (Kcal/mol)**	**Calculated K_i (μM)** *	**Tubulin residues involved in ligand binding** §	
5	-7.77	2.0	**Asp β179, Gln β394**	*Ala α314, Cys* α347, *Pro α348, Pro β173, Pro β175, Val β181, Pro β184*
6	-8.17	1.02	**Asp β179, Gln β394**	*Ala α314, Cys* α347, *Pro α348, Pro β173, Pro β175, Val β181, Pro β184*
7	-9.48	0.113	**Asp β179, Gln β394**	*Ala α314, Cys* α347, *Pro α348, Pro β173, Pro β175, Val β181, Pro β184*
8	-7.13	5.99	**Asp β179**	*Ala α314, Cys* α347, *Pro α348, Pro β173, Pro β175, Val β181, Pro β184*
9	-8.80	0.357	**Asp β179**	*Ala α314, Cys* α347, *Pro α348, Pro β173, Pro β175, Val β181, Pro β184*
10	-7.25	4.86	**Asp β179**	*Ala α314, Cys* α347, *Pro α348, Pro β173, Pro β175, Val β181, Pro β184*
11	-6.18	29.57	**Asp β179, Gln β394**	*Pro α348, Pro β173, Pro β175, Pro β184*
12	-6.33	23.03	**Asp β179, Gln β394**	*Pro α348, Pro β173, Pro β175, Pro β184*
13 +	-6.04	37.52	**Gln β11, Gln β15**	*Leu β209, Leu β227*

* K_i values as calculated by Autodock algorithm: $K_i = \exp(\Delta G/(R*T)$

§ Residues involved in Hydrogen bond are listed in **bold**. Hydrophobic contacts in *Italic.*

+ Binds in a different cleft, on the surface of the beta subunit, out from the dimeric interface

Based on the geometry, the binding energy and the clusterization of the results, we selected as best candidates, molecules **7**, **6** and **9** in ranked order.

FIGURE 9

3. Conclusions

Over the last years, the indole-based compounds have occupied an important position as powerful and versatile pharmacological weapons in the battle against life-threatening diseases as, for instance, cancer. Indeed, several indole derivatives have been employed pre-clinically and clinically and their multi-target features offered better and more promising therapies, overcoming the drug resistance mechanism and diminishing the undesirable side effects. The assessment of the basic importance of cancer microenvironment have enlarged the number of potential targets hit by indole derivatives and drugs that can control the microtubule assembly by hampering tubulin polymerization or, as well, by obstructing microtubule disassembly, and it could represent pivotal leads to block cancer metastasization. In this paper, we reported the design, the synthesis and the biological evaluation of molecules bearing the indole scaffold. Structure-activity relationships were made, based on the antitumor activities obtained against four cancer cell models (MCF-7, MDA-MB-231, HeLa and Ishikawa). We selected a good lead compound with no effects on the viability of three different normal cells. We proved that compound **7** is able to kill selectively the cancer cells, used in these experiments, by blocking the tubulin polymerization reaction, as demonstrated by a direct enzymatic assay and immunostaining studies on the native tubulin. Finally, *in silico* studies corroborated the observed tubulin inhibition. Targeting tubulin, compound **7** lead to cancer cells death by inducing apoptosis. Moreover, we studied the antioxidant properties of this series, finding out that compound **7** can reduce the menadione-induced ROS production in 3T3-L1 cells and that compound **6**, **9** and **10** showed the greatest scavenging activity in DPPH and ABTS assays. We are confident that these

outcomes will be exploitable for a better understanding of the great potential of indole derivatives as anticancer drugs.

4. Experimental Protocols

4.1. Chemistry

Chemicals were purchased from Sigma-Aldrich or Lancaster. Yields refer to purified products and were not optimized. Compound structures were confirmed by routine spectrometric and spectroscopic analyses. Melting points were determined on a Gallenkamp melting point apparatus in open glass capillary tubes and are uncorrected. The infrared spectra were recorded on a Perkin-Elmer (Norwalk, CT) Spectrum One FT spectrophotometer and band positions are given in reciprocal centimetres (cm^{-1}). ^{1}H NMR and ^{13}C NMR spectra were recorded on a Varian Mercury-VX spectrometer operating at 300 and 75 MHz for ^{1}H and ^{13}C, respectively using $CDCl_3$ or DMSO-d_6 as solvents. Chemical shifts are reported in parts per million (ppm) relative to solvent resonance: δ 7.26 (^{1}H NMR) and δ 77.3 (^{13}C NMR); DMSO-d_6, δ 2.48 (^{1}H NMR) and δ 40.3 (^{13}C NMR). *J* values are given in Hz. EI mass spectra were recorded on a Hewlett-Packard 6890-5973 MSD gas chromatograph/mass spectrometer at low resolution. Elemental analyses (C, H, N) were used to confirm the purity of all new compounds and were performed on a Eurovector Euro EA 3000 analyser (results within ± 0.4 of the theoretical values). Chromatographic separations were performed on silica gel columns by flash chromatography (Kieselgel 60, 0.040–0.063 mm, Merck, Darmstadt, Germany). TLC analyses were performed on precoated silica gel on aluminium sheets (Kieselgel 60 F254, Merck).

Synthesis of 5-methoxy-1-methylindole (2). To a stirred cold solution (0 °C) of 5-methoxyindole (**1**) (2.0 g, 13.6 mmol) in dry DMF (60 mL), NaH 60% oil dispersion (0.54 g, 20.4 mmol) was added. After 15 min, iodomethane (2.54 mL, 40.8 mmol) was added and the mixture was further stirred at room temperature for 1 h. Water (200 mL) was then added to the reaction mixture and the solid product obtained was filtered, washed with water and dried to give 2.7 g of pure **2** as a white solid.

Yield: 81%; mp: 114–115 °C; GC/MS (70 eV) m/z (%): 161 (M^+, 100). Spectroscopic data were in agreement with the literature[10].

Synthesis of 5-hydroxy-1-methylindole (3). A mixture of 5-methoxy-1-methylindole (**2**, 1.0 g, 6.21 mmol) and anhydrous pyridine hydrochloride (17.9 g, 156 mmol) was heated to reflux for 3 h. The reaction mixture was left to cool to room temperature, then ice water was added. The product was extracted with Et_2O. The organic layers were washed with a solution of HCl 2 N, dried (Na_2SO_4) and concentrated to give 0.37 g of **3** as a yellow solid. Yield: 46%; mp: 130–132 °C; lit.[120] 156 °C; GC/MS (70 eV) m/z (%): 147 (M^+, 100). Spectroscopic data were in agreement with the literature[10].

Synthesis of 1H-indol-5-yl pent-2-ynoate (5). To a stirred solution of 5-hydroxyindole (**4**, 0.30 g, 2.3 mmol) in a mixture of CH_2Cl_2 and DMF (10+1 ml), pent-2-ynoic acid (0.24 g, 2.5 mmol), dicyclohexylcarbodiimide (0.47 g, 2.3 mmol) and dimethyl aminopyridine (0.024 g, 0.2 mmol) were added. The reaction mixture was stirred at room temperature for 4 h, and then concentrated under reduced pressure. The solid residue was suspended in ethyl acetate, filtered and the filtrate was washed with brine. The organic layer was dried over anhydrous Na_2SO_4 and evaporated under reduced pressure. The solid residue was purified by silica gel chromatography (ethyl acetate/hexane 2:8) to give 0.24 g (48%) of a white solid: mp 116–117 °C; IR (KBr): 3386 (NH), 2231 (C≡C), 1706 (C=O) cm^{-1}; ^1H NMR (500 MHz, $CDCl_3$): δ 1.25 (t, *J* = 7.3 Hz, 3H, C*H*$_3$), 2.41 (q, *J* = 7.3 Hz, 2H, C*H*$_2$), 6.52 (s, 1H, Ar), 6.93 (dd, *J* = 8.8, 2.4 Hz, 1H, Ar), 7.18 (t, *J* = 2.4, 8.8 Hz, 1H, Ar), 7.28 (d, *J* = 8.8 Hz, 1H, Ar), 7.37 (d, *J* = 1.9 Hz, 1H, Ar), 8.28 (br s, 1H, N*H*); ^{13}C NMR (125 MHz, $CDCl_3$): δ 12.5 (1C), 72.4 (1C), 77.0 (1C), 92.9 (1C), 102.8 (1C), 111.5 (1C), 112.5 (1C), 115.7 (1C), 125.8 (1C), 128.0 (1C), 133.9 (1C), 143.7 (1C), 153.3 (1C); MS (70 eV) *m/z* (%) 213 (M^+, 39), 133 (100). Anal. ($C_{13}H_{11}NO_2.0.25H_2O$) C, H, N.

Synthesis of 1H-indol-5-yl hex-2-ynoate (6). Prepared as reported for **5** starting from 5-hydroxyindole (**4**) and es-2-ynoic acid. Light brown solid. Yield: 42%; mp 82–83 °C; IR (KBr): 3394 (NH), 2228 (C≡C), 1708 (C=O) cm^{-1}; ^1H NMR (500 MHz, $CDCl_3$): δ 1.04 (t, *J* = 7.3 Hz, 3H, C*H*$_3$), 1.61–1.68 (m, 2H, C*H*$_2$), 2.37 (t, *J* = 7.3 Hz, 2H, C*H*$_2$), 6.52 (s, 1H, Ar), 6.93 (dd, *J* = 8.8, 2.4 Hz,

1H, Ar), 7.19 (t, *J* = 2.9 Hz, 1H, Ar), 7.29 (d, *J* = 8.8 Hz, 1H, Ar), 7.37 (d, *J* = 1.9 Hz, 1H, Ar), 8.27 (br s, 1H, N*H*); ^{13}C NMR (125 MHz, $CDCl_3$): δ 13.5 (1C), 20.9 (1C), 73.1 (1C), 77.0 (1C), 91.8 (1C), 102.9 (1C), 111.5 (1C), 112.6 (1C), 115.7 (1C), 125.7 (1C), 128.0 (1C), 133.8 (1C), 143.8 (1C), 153.3 (1C); MS (70 eV) *m/z* (%) 227 (M^+, 81), 133 (100). Anal. ($C_{14}H_{13}NO_2$) C, H, N.

Synthesis of 9-ethylpyrano[3,2-e]indol-7(3H)-one (11). To a solution of **5** (0.25 g, 1.17 mmol) in a mixture of 1,4-dioxane and 1,2-dichloroethane (6+6 ml), $PtCl_4$ (0.02 g, 0.06 mmol) was added. The reaction mixture was heated under reflux for 4 h then concentrated under reduced pressure. The residue was dissolved in ethyl acetate and washed with water and brine. The organic layer was then dried (Na_2SO_4) and concentrated under reduced pressure to give a solid residue. The solid product was purified by silica gel chromatography (ethyl acetate/hexane 1:1) to give 40 mg (55%) of a ochre-yellow solid: mp 242–243 °C; IR (KBr): 3253 (NH), 1671 (C=O) cm^{-1}; ^{1}H NMR (500 MHz, DMSO-d_6): δ 1.3 (t, *J* = 7.3 Hz, 3H, CH_3), 3.08 (q, *J* = 7.3 Hz, 2H, CH_2), 6.24 (s, 1H, Ar), 6.83 (s, 1H, Ar), 7.14 (d, *J* = 8.3 Hz, 1H, Ar), 7.59 (t, *J* = 2.9 Hz, 1H, Ar), 7.68 (d, *J* = 8.3 Hz, 1H, Ar), 11.7 (br s, 1H, N*H*); ^{13}C NMR (125 MHz, DMSO-d_6): δ 12.7 (1C), 25.7 (1C), 27.9 (1C), 31.1 (1C), 70.2 (1C), 103.0 (1C), 111.2 (1C), 116.7 (1 C), 122.2 (1C), 128.2 (1C), 129.2 (1C), 131.9 (1C), 133.2 (1C); MS (70 eV) *m/z* (%) 213 (M^+, 87), 170 (100). Anal. ($C_{13}H_{11}NO_2 \cdot 0.34\ H_2O$) C, H, N.

Synthesis of 9-propylpyrano[3,2-e]indol-7(3H)-one (12). Prepared as reported for **11** starting from **6.** Ochre-yellow solid. Yield: 16%; mp 234–235 °C; IR (KBr): 3188 (NH), 1667 (C=O) cm^{-1}; ^{1}H NMR (500 MHz, DMSO-d_6): δ 1.03 (t, *J* = 7.3 Hz, 3H, CH_3), 1.66–1.74 (m, 2H, CH_2), 2.98 (t, *J* = 7.3 Hz, 2H, CH_2), 6.23 (s, 1H, Ar), 6.75 (d, *J* = 1.9 Hz, 1H, Ar), 7.13 (d, *J* = 8.8 Hz, 1H, Ar), 7.59 (t, *J* = 2.9 Hz, 1H, Ar), 7.68 (d, *J* = 8.8 Hz, 1H, Ar), 11.7 (br s, 1H, N*H*); ^{13}C NMR (125 MHz, DMSO-d_6): δ 14.0 (1C), 21.3 (1C), 36.6 (1C), 102.7 (1C), 111.2 (1C), 111.3 (1C), 112.3 (1C), 116.7 (1C), 122.2 (1C), 128.2 (1C), 133.3 (1C), 150.1 (1C), 158.6 (1C), 160.9 (1C); MS (70 eV) *m/z* (%) 227 (M^+, 100). Anal. ($C_{14}H_{13}NO_2 \cdot 0.34\ H_2O$) C, H, N.

Synthesis of 1H-indol-5-yl 3-phenylprop-2-ynoate (7). Prepared as reported for **5** starting from 5-hydroxyindole (**4**) and phenylpropiolic acid. Light beige solid. Yield: 40%; mp 142–143 °C; IR

(KBr): 3409 (NH), 2221 (C≡C), 1705 (C=O) cm^{-1}; ^1H NMR (500 MHz, $CDCl_3$): δ 6.56 (s, 1H, Ar), 7.0 (dd, *J* = 8.8, 1.9 Hz, 1H, Ar), 7.24 (q, *J* = 3.9 Hz, 1H, Ar), 7.36–7.44 (m, 3H, Ar), 7.47 (q, *J* = 7.3 Hz, 2H, Ar), 7.62 (d, *J* = 7.8 Hz, 2H, Ar), 8.26 (br s, 1H, N*H*); ^{13}C NMR (125 MHz, $CDCl_3$): δ 76.7 (1C), 77.0 (1C), 77.2 (1C), 80.6 (1C), 88.3 (1C), 103.0 (1C), 111.5 (1C), 112.7 (1C), 115.8 (1 C), 119.4 (1C), 125.7 (1C), 128.1 (1C), 128.6 (1C), 130.9 (1C), 133.1 (1C), 133.9 (1C), 143.8 (1C), 153.4 (1C); MS (70 eV) *m/z* (%) 261 (M^+, 23), 129 (100). Anal. ($C_{17}H_{11}NO_2 \cdot 0.17\ H_2O$) C, H, N.

Synthesis of 1-methyl-1H-indol-5-yl pent-2-ynoate (8). Prepared as reported for **5** starting from 5-methoxyindole (**3**) and pent-2-ynoic acid. Tan solid. Yield: 40%; mp 47–48 °C; IR (KBr): 2221 (C≡C), 1723 (C=O) cm^{-1}; ^1H NMR (300 MHz, $CDCl_3$): δ 1.25 (t, *J* = 1.1 Hz, 3H, CH_2CH_3), 2.40 (q, *J* = 6.4 Hz, 2H, CH_2), 3.80 (s, *J* = 1.1 Hz, 3H, NCH_3), 6.46 (d, *J* = 2.9 Hz, 1H, Ar), 6.97 (dd, *J* = 8.7, 2.3 Hz, 1H, Ar), 7.08 (d, *J* = 2.9 Hz, 1H, Ar), 7.25–7.35 (m, 1H, Ar); ^{13}C NMR (75 MHz, $CDCl_3$): δ 12.5 (1C), 30.9 (1C), 33.0 (1C), 72.4 (1C), 76.9 (1C), 92.6 (1C), 101.2 (1C), 109.6 (1C), 112.8 (1C), 115.3 (1C), 128.5 (1C), 130.1 (1C), 134.8 (1C), 143.6 (1C); MS (70 eV) *m/z* (%) 227 (M^+, 41); 147 (100). Anal. ($C_{14}H_{13}NO_2 \cdot 0.20\ H_2O$) C, H, N.

Synthesis of 9-ethyl-3-methylpyrano[3,2-e]indol-7(3H)-one (13). Prepared as reported for **11** starting from **8**. Tan solid. Yield: 62%; mp 174–175 °C; IR (KBr): 1630 (C=O) cm^{-1}; ^1H NMR (300 MHz, $CDCl_3$): δ 1.41 (t, *J* = 7.0 Hz, 3H, CH_2CH_3), 3.13 (q, *J* = 5.8 Hz, 2H, CH_2), 3.87 (s, 3H, NCH_3), 6.32 (s, 1H, Ar), 6.82 (d, *J* = 4.1 Hz, 1H, Ar), 7.23–7.28 (m, 2H, Ar), 7.5 (d, *J* = 8.7 Hz, 1H, Ar); ^{13}C NMR (75 MHz, $CDCl_3$): δ 12.1 (1C), 28.0 (1C), 30.8 (1C), 33.2 (1C), 72.1 (1C), 100.4 (1C), 102.1 (1C), 111.7 (1C), 111.9 (1C), 113.3 (1C), 119.2 (1C), 130.4 (1C), 159.5 (1C), 163.4 (1C); MS (70 eV) *m/z* (%) 227 (M^+, 100). Anal. ($C_{14}H_{13}NO_2$) C, H, N.

Synthesis of 1-methyl-1H-indol-5-yl hex-2-ynoate (9). Prepared as reported for **5** starting from 5-methoxyindole (**3**) and es-2-ynoic acid. Slightly yellowish oil. Yield: 11%; ^1H NMR (300 MHz, $CDCl_3$): δ 1.04 (t, *J* = 7.0 Hz, 3H, CH_2CH_3), 1.65 (q, *J* = 7.0 Hz, 2H, CH_2CH_3), 2.37 (t, *J* = 7.0 Hz, 2H, CCH_2), 3.77 (s, 3H, NCH_3), 6.46 (d, *J* = 2.9 Hz, 1H, Ar), 6.97 (dd, *J* = 8.8, 2.3 Hz, 1H, Ar), 7.08 (d, *J* = 3.5 Hz, 1H, Ar), 7.29 (d, *J* = 8.8 Hz, 1H, Ar), 7.35 (d, *J* = 2.3 Hz, 1H, Ar); ^{13}C NMR (75 MHz,

$CDCl_3$): δ 13.4 (1C), 20.7 (1C), 21.0 (1C), 33.0 (1C), 73.1 (1C), 91.5 (1C), 101.2 (1C), 109.5 (1C), 112.8 (1C), 115.3 (1C), 128.5 (1C), 130.1 (1C), 134.8 (1C), 143.6 (1C), 153.1 (1C); MS (70 eV) *m/z* (%) 241 (M^+, 33), 147 (100).

Synthesis of 1-methyl-1H-indol-5-yl 3-phenylprop-2-ynoate (10). Prepared as reported for **5** starting from 5-methoxyindole (**3**) and phenylpropiolic acid. Brown oil. Yield: 34%; IR (NaCl): 2222 (C≡C), 1723 (C=O) cm^{-1}; ^{1}H NMR (500 MHz, $CDCl_3$): δ 3.79 (s, 3H, C*H*$_3$), 6.50 (s, 1H, Ar), 7.06 (d, *J* = 8.8 Hz, 1H, Ar), 7.10 (s, 1H, Ar), 7.32 (d, *J* = 8.8 Hz, 1H, Ar), 7.38–7.52 (m, 4H, Ar), 7.64 (d, *J* = 7.3 Hz, 2H, Ar); ^{13}C NMR (125 MHz, $CDCl_3$): δ 33.0 (1C), 80.6 (1C), 88.2 (1C), 101.3 (1C), 109.7 (1C), 112.8 (1C), 115.3 (1C), 119.5 (1C), 128.6 (1C), 128.7 (2C), 130.3 (1C), 130.8 (1C), 133.2 (2C), 134.9 (1C), 143.7 (1C), 153.5 (1C); MS (70 eV) *m/z* (%) 275 (M^+, 38), 129 (100).

4.1.2 Thermal stability test

20 mg of **7** were heated in a reaction flask in oil bath for 6 hours at 60 °C.

4.2 Biology

4.2.1 Cell culture

The six cell lines used in this work (MCF-7, MDA-MB-231, HeLa, ISHIKAWA, MCF-10A and HEK-293) were purchased from American Type Culture Collection (ATCC, Manassas, VA, USA). All cells lines were maintained at 37 °C in a humidified atmosphere of 95% air and 5% CO_2 and periodically screened for contamination. MCF-7, human breast cancer cells estrogen receptor (ER)-positive, and human breast cancer triple negative MDA-MB231 were grown in DMEM-F12 medium containing 2 mmol/L L-glutamine, 1 mg/mL penicillin-streptomycin and 5% Newborn Calf Serum (NCS) or 5% Fetal Bovine Serum (FBS), respectively. HeLa (human epithelial cervix carcinoma cells), estrogen receptor (ER)-negative, and Ishikawa (human endometrial adenocarcinoma cells), estrogen receptor (ER)-positive, were cultured in MEM (minimum essential Eagle's Medium) supplemented with 10% FBS, 1% L-glutamine, 100 U/mL penicillin/streptomycin and 1% Non-Essential Amino Acids (NEAA). MCF-10A human mammary epithelial cells were cultured in

DMEM/F12 medium, supplemented with 5% horse serum (HS) (Eurobio, Les Ullis, Cedex, France), 100 U/mL penicillin/streptomycin, 0.5 mg/mL hydrocortisone, 20 ng/mL hEGF (human epidermal growth factor), 10 mg/mL insulin and 0.1 mg/mL cholera enterotoxin (Sigma-Aldrich, Milano, Italy). HEK-293, human embryonic kidney cells, were cultured in DMEM high glucose supplemented with 10% FBS, 1% L-glutamine and 100 U/mL penicillin/streptomycin.

4.2.2 MTT assay

The *in vitro* antiproliferative activities of all the target compounds were determined by a MTT (Sigma) assay [21-22]. Briefly, approximately cells were seeded in a 48-well plate and were grown in full medium. Before being treated, cells have been starved in serum free medium for 24 h for allowing cell cycle synchronization. After cells were exposed to compounds of differing concentrations (0,1-1-10-20-40 μM) for 24 h. Then to the treatment cells, MTT (3-(4,5-dimethylthiazol-2-yl)-2,5-diphenyl tetrazolium bromide) was added to each well (final concentration (0.5 mg/mL), followed by incubation for 2 h at 37 °C. After incubation, the supernatant from each well was carefully removed and the formazan crystals were dissolved in 200 μL of DMSO and then optical density was measured at 570 nm using a microplate reader. Results are represented as percent (%) of basal and the IC_{50} values were calculated using GraphPad Prism 6 (GraphPad Software, La Jolla, CA, USA).

4.2.3 Cytoskeleton and mitochondrial staining and immunofluorescence

Cells were added in 48-well culture plates containing glass slides and allowed to attach overnight at 37 °C in 5% CO_2, then serum-deprived for 24h and exposed to compounds for 24h (concentration equal to its IC_{50} value). Then, the cells after PBS-washed, were fixed with cold methanol, for 15 min at -20°C, and incubated with primary antibody, diluted in blocking solution overnight at 4°C, as previously described[12]. The rabbit anti-β-Tubulin (9104) were purchased from Santa Cruz Biotechnology and used at 1:100 dilution. Coverslips were then washed 3 times with PBS, then the secondary antibody Alexa Fluor® 488 conjugate goat-anti-rabbit (1:500, Thermo Fisher Scientific,

MA, USA) was added and incubated for 2h at 37 °C. Nuclei were stained using DAPI (Sigma Aldrich, Mila, Italy) for 10 min at a concentration of 0.2 μg/mL then washed 3 times with PBS. Fluorescence was detected using a fluorescence microscope (Leica DM 6000). LAS-X software was used to acquire and process all images.

4.2.4 Tubulin polymerization assay

Tubulin polymerization inhibition was measured using *in vitro* Tubulin Polymerization Assay Kit purchased from EMD Millipore Corporation[14]. Polymerization reactions occur in 70 μL final volumes, of which 60 μL is the 60 μM tubulin in 1xPB-GTP and 10 μL is the test substance dissolved in 1 x PB-GTP. Paclitaxel, Vinblastine (used as control) and compound **7**, were dissolved in DMSO and used at final concentration of 10 μM. These reactive were combined in 96-well plate on ice. After the plate was transferred into the spectrophotometer pre-warmed at 37 °C and the turbidity variation was measured every 30 seconds at 350 nm for 90 minutes. The plate was shacked for 10 seconds before each measurement. Turbidity (absorbance) readings were used to calculate the extent of polymerization [% inhibition = (1−A350 sample/A350 control) × 100].

4.2.4 TUNEL assay

Apoptosis was detected by the TUNEL assay, according to the guidelines of the manufacturer (CF^{TM}488A TUNEL Assay Apoptosis Detection Kit, Biotium, Hayward, CA). The cells were grown on glass coverslips and, after treatment, they were washed trice with PBS, then methanol-fixed at -20 °C for 15 min. After three washes with 0.01% (v/v) Triton X-100 in PBS, they were incubated with 100 mL of TUNEL equilibration buffer for 5 min. After its removal, 50 mL of TUNEL reaction mixture containing 1 mL of terminal deoxynucleotidyl transferase (TdT) were added to each sample and incubated in a dark and humidified chamber for 2 h at 37 °C. Samples were washed three-times with ice-cold PBS containing 0.1% Triton X-100 and 5 mg/mL bovine serum albumin. DAPI (Sigma, 0.2 mg/mL) counterstain was performed for 10 min at 37 °C under dark and humidified conditions.

Fixed cells were then washed trice with cold PBS (0.5 mL), adding one drop of mounting solution, and were observed and imaged under a fluorescence microscope (Leica DM6000; 20x magnification) with excitation/emission wavelength maxima of 490/515 nm (CF 488A) or 350/460 nm (DAPI). Images are representative of three independent experiments.

4.2.5 Detection of intracellular H_2O_2

Cells were grown in 48-well plates and then co-treated with the tested compounds and with menadione (Sigma-Aldrich), used to induce ROS production [23]. After treatment, cells were washed with PBS and 10 μM 2´-7´-dichlorofluorescein diacetate (Sigma-Aldrich) was added for 40 min, and then incubated at 37 °C, 5% CO_2. In presence of intracellular H_2O_2, non-fluorescent 2´-7´-dichlorofluorescein diacetate (DCF-DA) is oxidized and converted to green fluorescent 2´,7´-dichlorofluorescein (DCF). Then, cells were fixed and processed, as already described [2]. At the end cells were observed and imaged under a fluorescence microscope (Leica DM6000; 20× magnification) with excitation/emission wavelength of 490 nm/515 nm (DCF) or 350 nm/460 nm (DAPI). Images are representative of three independent experiments. The increase or the decrease of ROS generation in the treated cells, shown as green fluorescence, was quantified using ImageJ.

4.3 Antioxidant activity

4.3.1 DPPH Assay

The free radical scavenging capacity of all compounds (**5–13**) was determined by DPPH assay according to a known protocol[24] at four different concentrations (2.5, 1.0, 0.5 and 0.1 mg mL^{-1} in DMSO)

More specifically, standard DMSO solutions (2.5, 1.0, 0.5 and 0.1 mg mL^{-1} DMSO) of all compounds were prepared. 0.1 mL of each solution was mixed with 0.1 mL of DPPH solution (1 mM in MeOH) and 2.8 mL of MeOH to give the final volume of 3 mL, so as to obtain four different solutions with concentrations of 8.33, 3.33, 1.67, 0.33 μg mL^{-1} for each compound. The mixtures were shaken

vigorously and incubated for 30 min at room temperature in the dark. The colorimetric decrease in absorbance of each sample was quantified spectrophotometrically at 517 nm against a blank (3 mL of MeOH) using a UV–vis spectrophotometer (model V-550, Jasco Europe). The control was a DPPH solution (2.8 mL of MeOH, 0.1 mL of DPPH 1 mM, 0.1 mL DMSO). Experiments were carried out in triplicate, and the results were expressed as a percentage of free radical inhibition ($\%I_{DPPH}$), according to the formula:

$$\%I_{DPPH} = \frac{\text{Absorbance517nm of control} - \text{Absorbance517nm of sample}}{\text{Absorbance517nm of control}} \text{ x } 100$$

The inhibition percentage values ($\%I_{DPPH}$) were used to calculate EC_{50} values by GraphPad Prism 8 software (GraphPad Inc., San Diego, CA). Trolox was used as the reference compound to build a calibration curve (33-0.003 μg mL^{-1}). and the results were also expressed as μg of Trolox Equivalent per gram of dry sample weight (μg TE/g DW) (TEAC).

4.3.2. ABTS Assay

The radical scavenging effects of all compounds on a 2,2'-azino-bis(3-ethylbenzothiazoline-6-sulfonate) radical cation ($ABTS^{\bullet+}$) were evaluated according to a known protocol[25].

Briefly, $ABTS^{\bullet+}$ radical stock solution was prepared by mixing 50 mL of 2 mM ABTS and 0.5 mL of 70 mM $K_2S_2O_8$ and allowing the solution to stand in the dark at room temperature for 16 h before use. The $ABTS^{\bullet+}$ solution was diluted with absolute ethanol to yield the absorbance of 0.70 ± 0.02 at 734 nm. Compounds solutions (2.5, 1.0, 0.5 and 0.1 mg mL^{-1} DMSO) were prepared and then 0.03 mL of each one was mixed with 3 mL of the $ABTS^{\bullet+}$ solution obtaining the final concentrations of 25, 10, 5, 1 μg mL^{-1}. Then the mixtures were kept in the dark and under stirring for 5 min before absorbance at 734 nm was measured. Experiments were carried out in triplicate. The control was an ABTS solution (0.03 mL of DMSO, 3 mL of ABTS).

The ABTS radical scavenging was expressed as ($\%I_{ABTS}$) compared to the control according to the formula:

$$\% I_{ABTS} = \frac{\text{Absorbance 734nm of control} - \text{Absorbance 734nm of sample}}{\text{Absorbance 734nm of control}} \times 100$$

E_{C50} values were calculated using GraphPad Prism 8 software (GraphPad Inc., San Diego, CA). Trolox was used as the reference compound to build a calibration curve and the results were expressed also as per gram of dry sample weight (μg TE/g DW) (TEAC).

4.3.4 ROS protection assay

For the evaluation of the protective role of the molecules against oxidative stress, 3T3-L1 mouse fibroblasts cells were grown in 48-well plates and then treated with the compounds to test, menadione (Sigma-Aldrich), which causes ROS production[23]. After treatment, cells were washed with PBS and 10 μM of 2´-7´-dichlorofluorescein diacetate (Sigma-Aldrich) was added for 40 min, and then incubated at 37 °C, 5% CO_2. In presence of intracellular H_2O_2, nonfluorescent 2´-7´-dichlorofluorescein diacetate (DCF-DA) is oxidized and converted to green fluorescent 2´,7´-dichlorofluorescein (DCF)[2]. Then, cells were washed with PBS and methanol-fixed at -20 °C for 15 min. After three washes with ice-cold PBS, 2-(4-amidinophenyl)-6- indole carbamidine dihydrochloride (DAPI; 0.2 mg mL^{-1}) counterstain was performed for 10 min at 37 °C under dark conditions. Cells were then washed three-times with cold PBS, one drop of mounting solution was added, and then they were observed and imaged under a fluorescence microscope (Leica DM6000; 20× magnification) with excitation/emission wavelength maxima of 490 nm/515 nm (DCF) or 350 nm/460 nm (DAPI). Images are representative of three independent experiments. The increase or the decrease of ROS generation in treated cells, shown as green fluorescence, was quantified using ImageJ.

4.4 Docking

Docking simulations were performed using the program Autodock v.4.2.2.[26]. All the simulations

were performed using the program defaults and a searching grid encompassing the whole protein volume. Each docking experiment consisted of 100 Lamarckian Genetic Algorithm runs. The generated docking poses were ranked in order of increasing docking energy values and clustered based on a RMSD cut-off value of 1.0 Å. From the structural analysis of the lowest energy solutions of each cluster, we could highlight the protein binding site. As targets for all the simulations we used: the molecular structure of the assembly formed by Tubulin α, Tubulin β, Stathmin4 and the Tubulin Tyrosine Ligase[20] [PDB code 5J2T]. Figure YY was drawn with the program Chimera[27].

Bibliography

[1] A. Fazio, D. Iacopetta, C. La Torre, J. Ceramella, N. Muia, A. Catalano, A. Carocci, M. S. Sinicropi, *Food & function* **2018**, *9*(12), 6618-6631.

[2] D. Iacopetta, F. Grande, A. Caruso, R. A. Mordocco, M. R. Plutino, L. Scrivano, J. Ceramella, N. Muia, C. Saturnino, F. Puoci, C. Rosano, M. S. Sinicropi, *Future medicinal chemistry* **2017**, *9*(17), 2011-2028.

[3] S. Dadashpour, S. Emami, *European journal of medicinal chemistry* **2018**, *150*, 9-29.

[4] B. P. Bandgar, L. K. Adsul, S. V. Lonikar, H. V. Chavan, S. N. Shringare, S. A. Patil, S. S. Jalde, B. A. Koti, N. A. Dhole, R. N. Gacche, A. Shirfule, *Journal of enzyme inhibition and medicinal chemistry* **2013**, *28*(3), 593-600.

[5] A. Brancale, R. Silvestri, *Medicinal research reviews* **2007**, *27*(2), 209-238.

[6] H. J. Park, H. J. Lee, E. J. Lee, H. J. Hwang, S. H. Shin, M. E. Suh, C. Kim, H. J. Kim, E. K. Seo, S. K. Lee, *Bioscience, biotechnology, and biochemistry* **2003**, *67*(9), 1944-1949.

[7] S. Adler, G. Rashid, A. Klein, *Anticancer research* **2011**, *31*(11), 3733-3737.

[8] D. Fanale, G. Bronte, F. Passiglia, V. Calo, M. Castiglia, F. Di Piazza, N. Barraco, A. Cangemi, M. T. Catarella, L. Insalaco, A. Listi, R. Maragliano, D. Massihnia, A. Perez, F. Toia, G. Cicero, V. Bazan, *Analytical cellular pathology* **2015**, *2015*, 690916.

[9] K. Sakchaisri, S. O. Kim, J. Hwang, N. K. Soung, K. H. Lee, T. W. Choi, Y. Lee, C. M. Park, N. R. Thimmegowda, P. Y. Lee, B. Shwetha, G. Srinivasrao, T. T. Pham, J. H. Jang, H. W. Yum, Y. J. Surh, K. S. Lee, H. Park, S. J. Kim, Y. T. Kwon, J. S. Ahn, B. Y. Kim, *PloS one* **2017**, *12*(3), e0173311.

[10] M. S. Sinicropi, A. Caruso, F. Conforti, M. Marrelli, H. El Kashef, J. C. Lancelot, S. Rault, G. A. Statti, F. Menichini, *Journal of enzyme inhibition and medicinal chemistry* **2009**, *24*(5), 1148-1153.

[11] I. B. Johns, E. A. McElhill, J. O. Smith, *J. Chem. Eng. Data* **1962**, *7*(2), 277-281.

[12] J. Ceramella, M. R. Loizzo, D. Iacopetta, M. Bonesi, V. Sicari, T. M. Pellicano, C. Saturnino, A. Malzert-Freon, R. Tundis, M. S. Sinicropi, *Food & function* **2019**, *10*(7), 4280-4290.

[13] R. Kaur, G. Kaur, R. K. Gill, R. Soni, J. Bariwal, *European journal of medicinal chemistry* **2014**, *87*, 89-124.

[14] D. Iacopetta, C. Rosano, M. Sirignano, A. Mariconda, J. Ceramella, M. Ponassi, C. Saturnino, M. S. Sinicropi, P. Longo, *Pharmaceuticals* **2020**, *13*(5).

[15] H. Aryapour, G. H. Riazi, S. Ahmadian, A. Foroumadi, M. Mahdavi, S. Emami, *Pharmaceutical biology* **2012**, *50*(12), 1551-1560.

[16] J. H. Hwang, M. Takagi, H. Murakami, Y. Sekido, K. Shin-ya, *Cancer letters* **2011**, *300*(2), 189-196.

[17] F. L. Kiechle, X. Zhang, *Clinica chimica acta; international journal of clinical chemistry* **2002**, *326*(1-2), 27-45.

[18] M. Redza-Dutordoir, D. A. Averill-Bates, *Biochimica et biophysica acta* **2016**, *1863*(12), 2977-2992.

[19] A. Floegel, D.-O. Kim, S.-J. Chung, S. I. Koo, O. K. Chun, *J Food Compos Anal* **2011**, *24*, 1043-1048.

[20] A. B. Waight, K. Bargsten, S. Doronina, M. O. Steinmetz, D. Sussman, A. E. Prota, *PloS one* **2016**, *11*(8), e0160890.

[21] D. Iacopetta, C. Rosano, F. Puoci, O. I. Parisi, C. Saturnino, A. Caruso, P. Longo, J. Ceramella, A. Malzert-Freon, P. Dallemagne, S. Rault, M. S. Sinicropi, *European journal of pharmaceutical sciences : official journal of the European Federation for Pharmaceutical Sciences* **2017**, *96*, 263-272.

[22] A. Fazio, C. La Torre, M. C. Caroleo, P. Caputo, P. Plastina, E. Cione, *Molecules* **2020**, *25*(4).

[23] D. N. Criddle, S. Gillies, H. K. Baumgartner-Wilson, M. Jaffar, E. C. Chinje, S. Passmore, M. Chvanov, S. Barrow, O. V. Gerasimenko, A. V. Tepikin, R. Sutton, O. H. Petersen, *The Journal of biological chemistry* **2006**, *281*(52), 40485-40492.

[24] P. Plastina, A. Apriantini, J. Meijerink, R. Witkamp, B. Gabriele, A. Fazio, *Nutrients* **2018**, *10*(6).

[25] M. Leporini, M. R. Loizzo, R. Tundis, C. La Torre, A. Fazio, P. Plastina, *Antioxidants* **2019**, *8*(6).

[26] G. M. Morris, R. Huey, W. Lindstrom, M. F. Sanner, R. K. Belew, D. S. Goodsell, A. J. Olson, *Journal of computational chemistry* **2009**, *30*(16), 2785-2791.

[27] E. F. Pettersen, T. D. Goddard, C. C. Huang, G. S. Couch, D. M. Greenblatt, E. C. Meng, T. E. Ferrin, *Journal of computational chemistry* **2004**, *25*(13), 1605-1612.